

We are IntechOpen, the world's leading publisher of Open Access books Built by scientists, for scientists

6,900

Open access books available

185,000

International authors and editors

200M

Downloads

Our authors are among the

154

Countries delivered to

TOP 1%

most cited scientists

12.2%

Contributors from top 500 universities



WEB OF SCIENCE™

Selection of our books indexed in the Book Citation Index
in Web of Science™ Core Collection (BKCI)

Interested in publishing with us?
Contact book.department@intechopen.com

Numbers displayed above are based on latest data collected.
For more information visit www.intechopen.com



Localization and Tracking Using Camera-Based Wireless Sensor Networks

J.R. Martínez-de Dios, A. Jiménez-González and A. Ollero
*Robotics, Vision and Control Research Group, University of Seville
Spain*

1. Introduction

This chapter presents various methods for object detection, localization and tracking that use a Wireless Sensor Network (WSN) comprising nodes endowed with low-cost cameras as main sensors. More concretely, it focuses on the integration of WSN nodes with low-cost micro cameras and describes localization and tracking methods based on Maximum Likelihood and Extended Information Filter. Finally, an entropy-based active perception technique that balances perception performance and energy consumption is proposed.

Target localization and tracking attracts significant research and development efforts. Satellite-based positioning has proven to be useful and accurate in outdoor settings. However, in indoor scenarios and in GPS-denied environments localization is still an open challenge. A number of technologies have been applied including inertial navigation (Grewal et al., 2007), ultra-wideband (Gezici et al., 2005) or infrared light signals (Depenthal et al., 2009), among others.

In the last decade, the explosion of ubiquitous systems has motivated intense research in localization and tracking methods using Wireless Sensor Networks (WSN). A good number of methods have been developed based on Radio Signal Strength Intensity (RSSI) (Zanca et al., 2008) and ultrasound time of flight (TOF) (Amundson et al., 2009). Localization based on Radio Frequency Identification (RFID) systems have been used in fields such as logistics and transportation (Nath et al., 2006) but the constraints in terms of range between transmitter and reader limits its potential applications. Note that all the aforementioned approaches require active collaboration from the object to be localized -typically by carrying a receiver- which imposes important limitations in some cases.

Also, recently, multi-camera systems have attracted increasing interest. Camera based localization has high potentialities in a wide range of applications including security and safety in urban settings, search and rescue, and intelligent highways, among many others. In fact, the fusion of the measurements gathered from distributed cameras can reduce the uncertainty of the perception, allowing reliable detection, localization and tracking systems. Many efforts have been devoted to the development of cooperative perception strategies exploiting the complementarities among distributed static cameras at ground locations (Black & Ellis, 2006), among cameras mounted on mobile robotic platforms (Shaferman & Shima, 2008) and among static cameras and cameras onboard mobile robots (Grocholski et al., 2006).

In contrast to other techniques, camera-based Wireless Sensor Networks, comprised of distributed WSN nodes endowed with a camera as main sensor, require no collaboration from the object being tracked. At the same time, they profit from the communication infrastructure, robustness to failures, and re-configurability properties provided by Wireless Sensor Networks.

This chapter describes various sensor fusion approaches for detection, localization and tracking of mobile objects using a camera-based Wireless Sensor Network. The main advantages of using WSN multi-camera localization and tracking are: 1) they exploit the distributed sensing capabilities of the WSN; 2) they benefit from the parallel computing capabilities of the distributed nodes; 3) they employ the communication infrastructure of the WSN to overcome multi-camera network issues. Also, camera-based WSN have easier deployment and higher re-configurability than traditional camera networks making them particularly interesting in applications such as security and search and rescue, where pre-existing infrastructure might be damaged.

This chapter is structured as follows:

- Section 2 includes a brief introduction to Wireless Sensor Networks and describes the basic scheme adopted for the camera-based WSN.
- Section 3 presents a basic data fusion based on Maximum Likelihood approach. The method has bad performance in case of losses of WSN messages, which can be not infrequent in some applications.
- Section 4 proposes a data fusion method based on Extended Information Filter. This method has good performance at moderate computer cost.
- Section 5 summarizes an entropy-based active perception technique that dynamically balances between perception performance and use of resources.
- Section 6, which describes implementation details and presents some experimental results.

Finally, Section 7 is devoted to the final discussions and conclusions.

2. Camera-based WSN

2.1 Brief introduction to wireless sensor networks

A Wireless Sensor Network (WSN) consists of a large number of spatially distributed devices (nodes) with sensing, data storage, computing and wireless communication capabilities. Low size, low cost and particularly low power consumption are three of the key issues of WSN technology. Nodes are designed to operate with minimal hardware and software requirements, see basic scheme of the main modules in Fig. 1Left. They often use 8 or 16-bit microcontrollers at low processing rates and a limited RAM capacity for data storage. Nodes often require a few milliwatts for operation. Most nodes can be set in a standby state, from which they wake up occasionally, for instance when one sensor detects an event. Their radio transceivers are also very energy efficient and their transmission range is typically less than 100 m in the open air. Besides, its bandwidth is often low.

In contrast to the simplicity of each node, the main strengths of WSN rely on the cooperation of a number of nodes for cooperatively performing tasks. In fact, a good number of algorithms have been developed to provide them significant flexibility, scalability, tolerance to failures and self-reconfiguration. WSN are typically organized in tree-like channels between data sources (nodes) and data sinks (WSN base), see Fig. 1Right. Despite this apparent simplicity, algorithms for network formation and information routing have been

intensively researched with the objective of optimizing the energy consumption, the communication delays expressed as the number of hops, the network dynamic reconfiguration or its reliability to failures. A survey on WSN routing protocols can be found in (Al-Karaki & Kamal, 2004).

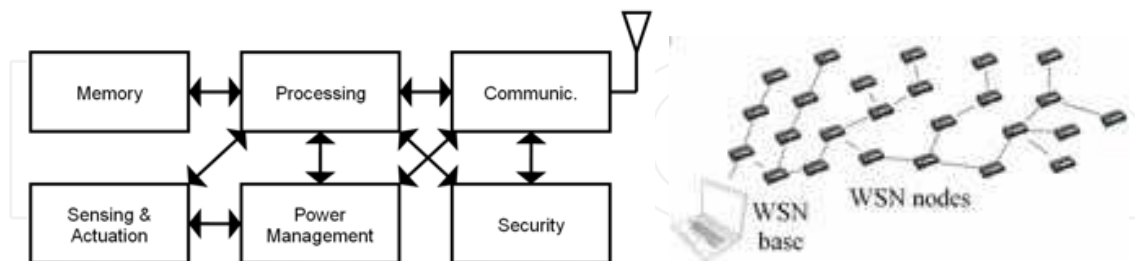


Fig. 1. Left) Basic module scheme of a WSN node. Right) Tree-like channels established in WSN between nodes (data sources) and the WSN base (data sink).

The nodes of the WSN can be equipped with a growing variety of sensors including light intensity sensors, optical barrier, presence sensors, gas sensors and GPS. These features together with battery operation facilitate its deployment with minimal invasion and low installation and maintenance costs. The standardization of communication protocols, such as IEEE 802.15.4, has facilitated the effort to extend its range of possible applications. WSN have already been applied to building control (Sandhu et al., 2004), environmental monitoring (Polastre et al., 2004) and manufacturing automation (Hansmann et al., 2008), among others (Akyildiz et al. 2002).

2.2 Camera-based WSN

A camera-based WSN uses cameras as main sensors of the distributed WSN nodes. In contrast to the advantage of using robust and reconfigurable WSN communication, camera-based WSN must face the main constraints of WSN technology, i.e. limited computational and data storage capacity and low communication bandwidth. Thus, centralized schemes in which all the images are processed by one node are not suitable for camera-based WSN. One proposed solution is to transmit the images gathered by the cameras through the WSN (Wark et al, 2007). However, this approach has bad scalability in terms of bandwidth, being critical in problems that require images of certain resolution at a certain rate. Also, additional constraints arise in centralized schemes when considering the computational and memory capacity required to process the images from all the cameras and fuse their results in only one WSN node. Lack of reliability to failures in the central node is another important drawback.

In our case a distributed scheme is adopted: the images captured by each camera are processed locally at each node. Camera nodes have sufficient computational capabilities to execute efficient image-processing algorithms in order to extract from the images the required information, for instance the location of an object on the image plane. Hence, only distilled bandwidth-reduced information from each camera node is transmitted through the WSN. Then, a node receiving the measurements from all the camera nodes can perform data fusion algorithms to determine the location of the object in real-world coordinates. This scheme reduces drastically the bandwidth requirements and distributes the overall computational burden among the nodes of the WSN.

In the adopted scheme, each camera node applies image-processing segmentation techniques to identify and locate the object of interest on the image plane. Thus, the possibility of flexibly programming image processing algorithms is a strong requirement. The selected camera board is the *CMUcam3*, an open source programmable board endowed with a color detector with 352x288 pixels. Figure 2 shows a picture of a camera node comprised of an *Xbow* node and one *CMUcam3* board.



Fig. 2. *CMUcam3* integrated with a *Xbow* node.

We implemented a robust algorithm based on a combination of color and motion segmentations capable of being efficiently executed with limited computational and memory resources. The result of the segmentation algorithm is a rectangular region on the image plane characterized by the coordinates of its central pixel, its width and height.

Several data fusion methods are used to merge the results from the segmentation algorithms running in every camera node. Data fusion reduces the influence of errors in measurements and increases the overall system accuracy. On the other hand, it requires having the measurements from all the cameras expressed in the same reference frame. In the methods presented, each camera node obtains the coordinates of the region of interest on the image plane applying image segmentation algorithms and corrects its own optical distortions transforming them to the undistorted normalized pin-hole projection on the image plane. Each camera is internally calibrated and the calibration parameters are known at each camera node. Hence, camera nodes message packets include the distortion-corrected normalized measurements for each image analyzed. These messages are transmitted through the WSN for data fusion. This approach standardizes the measurements from all camera nodes facilitating data fusion method and distributes the computational cost among the camera nodes. For further details of the implementations refer to Section 6.

3. Localization using maximum likelihood

Maximum Likelihood (ML) is one of the basic statistical data fusion methods, (Mohammad-Djafari, 1997). Its objective is to estimate the state of an event that best justifies the observations maximizing a statistical likelihood function that can be expressed as the probability of measurement z conditioned to state x :

$$\hat{x} = \arg \max_x \{P(z|x)\} \tag{1}$$

Assume that the state is measured synchronously from N different sensors z_1, \dots, z_N , where z_i is the measurement gathered by sensor i . Supposed the measurements of all the sensor z_1, \dots, z_N can be considered statistically independent, the overall likelihood function can be expressed by:

$$p(z_1, \dots, z_N | x) = \prod_{i=1}^N p(z_i | x) \tag{2}$$

Assume that each measurement is subject to errors that can be considered to be originated by the influence of a high number of independent effects. By virtue of the Central Limit Theorem it can be considered to have Gaussian distribution, (Rice, 2006):

$$p(z_i | x) = \det(2\pi\Sigma_i)^{-1/2} \exp \left\{ \frac{-1}{2} (z_i - x)^T \Sigma_i^{-1} (z_i - x) \right\} \tag{3}$$

where Σ_i is the covariance of measurements from sensor i . The ML method estimates the state as the following weighted sum:

$$x = (\Sigma_1^{-1} + \dots + \Sigma_N^{-1})^{-1} (\Sigma_1^{-1}z_1 + \dots + \Sigma_N^{-1}z_N) \tag{4}$$

where each measurement is weighted proportionally to the inverse of its covariance: measurements with more noise have lower weigh in (4). The overall estimated covariance follows the expression:

$$\Sigma_x = (\Sigma_1^{-1} + \dots + \Sigma_N^{-1})^{-1} \tag{5}$$

It should be noted that since $\Sigma_x < \Sigma_i$ the estimate is more accurate than any measure. The following describes the ML method adopted for camera-based WSN. Consider that a point P in the environment is observed by N camera nodes. $p_i = [x_i \ y_i]$ are the distortion-corrected pixel coordinates of P viewed from camera node i . Before applying (4) it is necessary to have the measurements from all the cameras in the same reference frame.

Let frame F_i be a reference frame local to camera i . The location and orientation of the N cameras in a global reference frame G are known. Let T_i be the transformation matrix from frame F_i to frame G . Assume that Z_i , the Z coordinate of P in frame F_i , is known. Taking into account the pin-hole model it is possible to project pixel p_i at distance Z_i :

$$P_i = [X_i \ Y_i \ Z_i]^T = [x_i Z_i \ y_i Z_i \ Z_i]^T \tag{6}$$

P_i represents the coordinates of P measured by camera i and expressed in frame F_i . Using T_i P_i can be transformed to frame G applying:

$$\begin{bmatrix} P_i^G \\ \mathbf{1} \end{bmatrix} = T_i^{-1} \begin{bmatrix} P_i \\ \mathbf{1} \end{bmatrix} \tag{7}$$

P_i^G represents the coordinates of P in frame G as measured by camera i . With the measurements from all the cameras in the same frame G , the ML method can be applied. Assume that P_i^G contains Gaussian errors with covariance matrix Σ_i . Supposed the measurements from different cameras statistically independent, the ML method estimates P with measurements P_i^G using (4).

Σ_i can be decomposed in an eigenvector matrix and an eigenvalue matrix, $\Sigma_i = L\Lambda L^{-1}$. The eigenvectors of Σ_i form the columns of L . The eigenvectors are orthonormal vectors that represent the axes of frame F_i in the global frame G . Λ is a diagonal matrix. The elements of the diagonal are the eigenvalues of Σ_i , which are the variance associated to P_i^G at each axis of frame F_i . L and Λ , and thus Σ_i can be easily constructed knowing the orientation of camera i and estimating the noise in the measurements.

Figure 3 shows an illustration of the method with two cameras. The probability distribution of the measurements from *Camera1* and *Camera2* are represented in cyan color. The probability distribution of the fused estimate is in blue. The remarkable reduction in the covariance denotes an increment in the fused estimate.

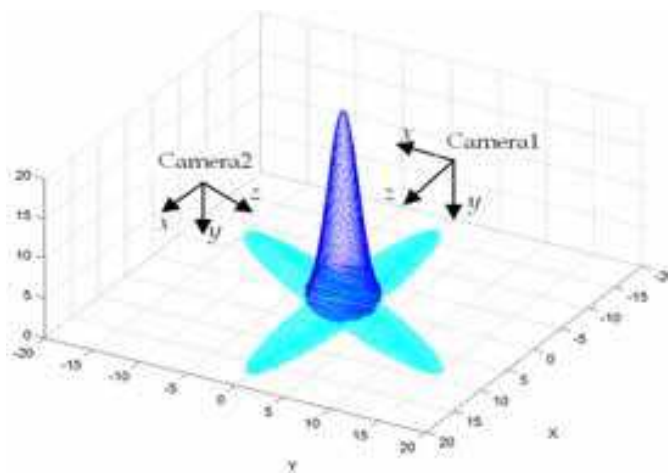


Fig. 3. Example illustrating ML data fusion method.

The described ML method can be executed in a WSN node in few milliseconds. This high efficiency facilitates schemes where camera nodes observing the same object interchange their observations and apply data fusion.

This method can be used for object localization but it is not suitable for object tracking, and even when used for localization the ML method has important constraints. Applying the ML data fusion requires having previously determined Z_i , the location of P in frame F_i . A typical approach is to set Z_i with an average value and compensate the error assuming a high value for the variance of the error at the Z axis of F_i . However, this artificial increase of uncertainty decreases the quality of the overall estimate. Another approach is to use, under an iterative scheme, the value of Z_i at time $t-1$. Nevertheless, this method requires assuming an initial value and, errors in estimation at time $t-1$ involve errors at subsequent iterations.

Furthermore, ML has high sensitivity to failures in measurements, for instance in cases where the object is out of the field of view of the camera, occluded in the image or in case of losses of WSN messages, not infrequent in some environments. This sensor fusion method relies totally on the measurements and its performance degrades when some of them are lost. Other sensor fusion techniques such as Bayesian Filters rely on observations and on models, which are very useful in case of lack of measurements.

4. Localization and tracking using EIF

Bayesian Filters (RBFs) provide a well-founded mathematical framework for data fusion. RBFs estimate the state of the system assuming that measurements and models are subject to uncertainty. They obtain an updated estimation of the system state as a weighted average using the prediction of its next state according to a system model and also using a new measurement from the sensor to update the prediction. The purpose of the weights is to give more trust to values with better (i.e., smaller) estimated uncertainty. The result is a new state estimate that lies in between the predicted and measured state, and has a better estimated uncertainty than either alone. This process is repeated every step, with the new estimate and measure of uncertainty used as inputs for the following iteration.

The Kalman Filter (KF) is maybe the most commonly used RBF method. The Kalman Filter and its dual, the Information Filter (IF), use a prediction model, that reflects the expected evolution of the state, and a measurement model, that takes into account the process through which the state is observed to respectively predict and update the system state:

$$\begin{aligned}x_t &= g(x_{t-1}) + \varepsilon_t \\z_t &= h(x_t) + \delta_t\end{aligned}\quad (8)$$

x_t is the current system state vector, x_{t-1} is the previous state vector, z_t is the measurement vector and ε_t and δ_t are White Gaussian Noise (WGN) parameterized by their mean value and a covariance matrix.

In our problem the measurements considered are the location of the object on the image of the distributed camera nodes. Even assuming simple pin-hole cameras, these observation models are non-linear and a first order linearization is required. In this case, having non-linear prediction and measurement models leads to the Extended Information Filter (EIF). After linearizing the IF equations via Taylor Expansion, we can assume that the predicted state probability, written as Gaussian, is as follows:

$$\begin{aligned}p(x_t | x_{t-1}) &= \det(2\pi R_t)^{-1/2} \\&\exp\left\{-\frac{1}{2}\left[(x_t - g(\mu_{t-1}) - G_t(x_{t-1} - \mu_{t-1}))\right]^T R_t^{-1} \left[(x_t - g(\mu_{t-1}) - G_t(x_{t-1} - \mu_{t-1}))\right]\right\}\end{aligned}\quad (9)$$

where μ_{t-1} is the mean of the previous state, R_t is the covariance of the prediction model (correspondent to ε_t) and G_t is the Jacobian matrix of g . The next state probability, written as Gaussian, is as follows:

$$\begin{aligned}p(z_t | x_t) &= \det(2\pi Q_t)^{-1/2} \\&\exp\left\{-\frac{1}{2}\left[(z_t - h(\bar{\mu}_t) - H_t(x_t - \bar{\mu}_t))\right]^T Q_t^{-1} \left[(z_t - h(\bar{\mu}_t) - H_t(x_t - \bar{\mu}_t))\right]\right\}\end{aligned}\quad (10)$$

where $\bar{\mu}_t$ is the mean of the predicted state, Q_t is the covariance of the measurement model (correspondent to δ_t) and H_t is the Jacobian matrix of h .

Information Filters (IF) employ the so-called *canonical representation*, which consists of an information vector $\xi = \Sigma^{-1}\mu$ and matrix $\Omega = \Sigma^{-1}$. Figure 4 shows the full EIF algorithm. In each recursive iteration it computes the current system state (ξ_t, Ω_t) from the previous state and

the new measurement $(\xi_{t-1}, \Omega_{t-1}, z_t)$. Each iteration is divided in two steps: prediction (lines 1-4 in Fig. 4) and update (lines 5, 6). For more details, refer to (Thrun et al., 2005).

Since both g and h require the state as an input, it is mandatory to recover the state estimate μ from canonical parameters (see step 1 of the EIF algorithm in Fig. 4) which makes the prediction stage from the algorithm lose efficiency compared to the EKF. Nevertheless, the update stage of EIF is much more efficient than EKF and thus the former is more suitable when there are a large number of observations. In this sense, the efficiency of this algorithm with respect to other implementations is improved when a simple prediction model together with a large measurement vector z_t are used. Besides, Information Filters are also numerically more stable and are more suitable for characterizing and representing information and its absence, $\Omega=0$.

Extended_Information_Filter $(\xi_{t-1}, \Omega_{t-1}, z_t)$:	
1:	$\mu_{t-1} = \Omega_{t-1}^{-1} \xi_{t-1}$
2:	$\bar{\Omega}_t = (G_t \Omega_{t-1}^{-1} G_t^T + R_t)^{-1}$
3:	$\bar{\xi}_t = \bar{\Omega}_t g(\mu_{t-1})$
4:	$\bar{\mu}_t = g(\mu_{t-1})$
5:	$\Omega_t = \bar{\Omega}_t + H_t^T Q_t^{-1} H_t$
6:	$\xi_t = \bar{\xi}_t + H_t^T Q_t^{-1} [z_t - h(\bar{\mu}_t) + H_t \bar{\mu}_t]$
7:	return ξ_t, Ω_t

Fig. 4. EIF algorithm.

Therefore, the selection of the state and models has critical impact on the performance and computational burden of the filter. We selected a state vector typical in tracking problems that considers only the current object position and velocity $x_t = [X_t \ Y_t \ Z_t \ Vx_t \ Vy_t \ Vz_t]^T$. In our problem we can have a large number of inexpensive camera nodes. We preferred EIF over EKF due to its better scalability with the number of observations. Also, we assumed a very simple local linear motion model to reduce the burden of the prediction stage in EIF:

$$\begin{cases} X_t = X_{t-1} + Vx_{t-1} \\ Y_t = Y_{t-1} + Vy_{t-1} \\ Z_t = Z_{t-1} + Vz_{t-1} \end{cases} \quad \begin{cases} Vx_t = Vx_{t-1} \\ Vy_t = Vy_{t-1} \\ Vz_t = Vz_{t-1} \end{cases} \quad (11)$$

Of course, we do not know a priori what kind of movement would the object perform. So we assume local linear motion and we include Gaussian noise in each coordinate to consider errors in the model. This model can efficiently represent local motions and has been extensively applied in RBFs. Also, more complex models increase the computation burden and would require a priori knowledge of the motion, unavailable in tracking of objects with no collaboration, as is the case of security applications.

The EIF uses a different observation model for each camera that is seeing the object. The observation model adopted for camera i uses as measurements the distortion-corrected pin-hole projections from camera i at time t , $p_{i,t}$. To allow the estimation of the object velocity, we

also include in the measurement the projection from camera i at time $t-1$, $p_{i,t-1}$. The measurement vector including measurements from all the N cameras that are tracking the object can be written as $z_t = [p_{1,t} \ p_{1,t-1} \ p_{2,t} \ p_{2,t-1} \ \dots \ p_{N,t} \ p_{N,t-1}]^T$.

The location of the object at time t in the global reference frame G , P_t , can be computed from $p_{i,t}$, its projection in the image plane of camera node i , as described in (6) and (7). Provided T_i is the transformation matrix of F_i , the reference frame of camera i , and $t_{i,j}$ represents the j -th row of T_i , the measurement from each camera node i can be related to the target position as:

$$p_{i,t} = \begin{bmatrix} x_{i,t} \\ y_{i,t} \end{bmatrix} = \begin{bmatrix} t_{i,1}[P_t \ 1]^T / t_{i,3}[P_t \ 1]^T \\ t_{i,2}[P_t \ 1]^T / t_{i,3}[P_t \ 1]^T \end{bmatrix} \quad (12)$$

Thus, the overall measurement model h which relates z_t with x_t can be written as:

$$h = [h_{1,t} \ h_{1,t-1} \ \dots \ h_{N,t} \ h_{N,t-1}]^T, \quad h_{i,t} = \begin{bmatrix} t_{i,1}[X_t \ Y_t \ Z_t \ 1]^T / t_{i,3}[X_t \ Y_t \ Z_t \ 1]^T \\ t_{i,2}[X_t \ Y_t \ Z_t \ 1]^T / t_{i,3}[X_t \ Y_t \ Z_t \ 1]^T \end{bmatrix} \quad (13)$$

This observation model is, as already stated, non-linear. At the updating stage the EIF requires using the Jacobian matrices of h , H_t .

Each measurement at each camera node i requires only one prediction step and one updating step. Assuming 3 cameras, the execution of an iteration of an EIF for 2D localization and tracking with 3 cameras requires approximately 6,000 floating point operations, roughly 400 ms. in a Xbow TelosB mote, such as those used in the experiments. The Bayesian approach provides high robustness in case of losses of measurements. If at time t there are no measurements, only the prediction stage of the EIF algorithm is executed. In this case, the uncertainty of the state grows more and more until new measurements are available. This behavior naturally increases the robustness in case of failures of the segmentation algorithm or losses of measurement messages. Thus, EIF exhibits higher robustness than ML to noisy measurements and particularly to the lack of measurements. Some experimental results can be found in Section 7.

5. Active perception techniques

In the previous schemes all the cameras that are seeing the object at any time t are used for data fusion regardless of the usefulness of the measurement they provide for the overall estimation. In this section we briefly summarize an entropy-based active perception approach that dynamically activates or deactivates each camera node balancing the information it effectively provides and the cost of the measurement.

The active perception problem can be broadly defined as the procedure to determine the best actions that should be performed. In our problem there are two types of actions, activate or deactivate camera i . Given a certain system state x , each action a involves an impact on the perception, i.e. it obtains a certain reward $r(x,a)$. Also, each action has a certain cost $c(x,a)$. For instance, by activating camera node i , the reward is a perception with lower uncertainty, and the cost is the increase of energy consumption.

In most active perception strategies the selection of the actions is carried out using reward VS cost analyses. In the so-called greedy algorithms the objective is to decide the next best action to be carried out without taking into account long-term goals. POMDPs (Kaelbling et

al., 1998), on the other hand, consider the long-term goals providing an elegant way to model the interaction of an agent in an environment, both of them uncertain. Nonetheless, POMDPs require intense computing resources and memory capacity. POMDPs also scale badly with the number of camera nodes. Thus, in our problem we adopted an efficient greedy active perception scheme.

At each time step, the strategy adopted activates or deactivates one camera node taking into account the expected information gain and the cost of the measurement. In our approach the reward is the information gain about the target location due to the new observation. Shannon entropy is used to quantify the information gain.

Consider the prior target location distribution at time t to be $p(x_t)$. If camera node i , currently unused, is activated and its measurement is available at t , then the posterior target location distribution will be $p(x_t | z_i)$. Then, the gain of information from activating camera node i can be expressed by $H(x_t) - H(x_t | z_i)$, where $H(x_t)$ and $H(x_t | z_i)$ stand for the Shannon entropy of $p(x_t)$ and $p(x_t | z_i)$. $H(x_t) - H(x_t | z_i)$ also denotes the mutual information between x_t and z_i .

Entropy is a measure of the uncertainty associated to a random variable, i.e. the information content missing when one does not know the value of a random variable. The reward for action $a=A(i)$ -activating camera node i - is expressed by:

$$r(x_t, a = A(i)) = H(x_t) - H(x_t | z_i) \quad (14)$$

There are analytical expressions to express the entropy of a Gaussian distribution. Assuming $p(x_t)$ and $p(x_t | z_i)$ are Gaussians the reward of an action can be computed with:

$$r(x_t, a = A(i)) = \frac{1}{2} \log \left(\frac{|\Sigma_1|}{|\Sigma_2|} \right) \quad (15)$$

where Σ_1 and Σ_2 are the covariance matrices of distributions $p(x_t)$ and $p(x_t | z_i)$.

On the other hand, the cost of activating a camera node is mainly expressed in terms of the energy consumed by camera. However, note that there are other costs, as those associated to the use of the wireless medium for transmitting the new measurements or the increase in computational burden required to consider the measurements from the new camera in the EIF. Also, these costs can vary depending on the camera node and the currently available resources. For instance, the cost of activating a camera with low battery level is higher than activating one with full batteries.

An action a_j is defined as advantageous at certain time t if the reward is higher than the cost, i.e. $r(x_t, a_j) > c(x_t, a_j)$. In a system with a set of potential advantageous actions, $a \in A^+$, the more advantageous action is selected to be carried out:

$$\hat{a} = \arg \max_{a_j \in A^+} \left(r(x_t, a_j) - c(x_t, a_j) \right) \quad (16)$$

This active perception method can be easily incorporated within a Bayesian Recursive Filter. In our case it was integrated in the EIF described in Section 5. To simplify the complexity and computer burden, the number of actions that can be done at each time is limited to one. Thus, in a deployment with N cameras the number of actions analyzed at each time is N : deactivation of each of the currently active camera nodes and activation of each of the currently unused camera nodes. The most advantageous action is selected to be carried out.

The main disadvantage of (14) is that the action to be carried out should be decided without actually having the new measurement. We have to rely on estimations of future information gain. At time t the information matrix of the EIF at t is Ω_t . In the prediction stage the information matrix is predicted, $\bar{\Omega}_{t+1}$, see the EIF algorithm in Fig. 4. In the update stage, it is updated, Ω_{t+1} , using the observation models of the sensors currently used. In case of performing sensory action a , the observation model would change and involve a new updated information matrix Ω_{t+1}^a . The expectation of the information gain can be approximated by $\frac{1}{2} \log(|\Omega_{t+1}^a| / |\Omega_{t+1}|)$.

This expression assumes that the location distribution of the target is Gaussian, which is not totally exact due to the nonlinearities in the observation pin-hole models. Also, they provide expectation of the information gain instead of the information gain itself. Despite these inaccuracies, it is capable of providing a useful measure of the information gain from a sensory action in an efficient way. In fact, the active perception method for a setting with 3 cameras adopted requires approximately 3,400 floating point operations, roughly 300 ms in Xbow TelosB motes, but can imply remarkable resources saving rates, up to 70% in some experiments shown in Section 6. It should be noted that its computational burden scales well since it is proportional to the number of cameras in the setting.

6. Implementation and some results

This Section provides details of the camera-based WSN implementation and presents some experimental results.

6.1 Implementation of camera-based WSN with COTS equipment

Requirements such as energy consumption, size and weight are very important in these systems. In our experiments we used *TelosB* motes from *Xbow Inc* (<http://www.xbow.com>). These motes use a *Texas Instruments* MPS430 16-bit microprocessor at 8 MHz, which can be enough to execute algorithms with low computer-burden but is not capable of applying image processing methods with sufficient image resolution and frame rate. The RAM memory of *TelosB* (10 KB) is also insufficient for most image processing techniques. In previous developments we also used *Xbow Mica2* motes, with lower resources.

The micro camera board selected is the *CMUcam3* (<http://www.cmucam.org>). It is an open source programmable embedded platform connected to an *Omnivision* 1/4" CMOS 352x288 color detector. Its main processor, the *NXP LPC2106*, allows implementing, in Custom C, code-efficient real-time image processing algorithms. Different lenses (of up to 150° FOV_H) were used in the experiments to accommodate the dimensions of the environment. Figure 5 shows a set of camera nodes. They were mounted on small tripods to facilitate deployment and orientation. In preliminary works we used *CMUcam2* boards. The main practical advantages of *CMUcam3* over *CMUcam2* are the possibility of being programmed (*CMUcam2* used fixed pre-programmed algorithms instead) and a high reduction in energy consumption.

Each *CMUcam3* is connected to a single *Xbow* mote through a RS-232 link. The *CMUcam3* board captures the images and executes the algorithms for object segmentation while the *Xbow* mote runs a series of algorithms required for cooperative location and tracking including control of the *CMUcam3*, correction of optical distortions, algorithms for synchronization among the camera nodes and wireless transmission of the measurements. From the *Xbow* side, *CMUcam3* operates transparently as any other sensor.



Fig. 5. Set of camera nodes equipped with *CMUcam2* and *CMUcam3* micro cameras.

6.1.1 Image segmentation

Although *CMUcam3* offers programming facilities, its limited computational and memory resources require efficient algorithm design and coding to achieve near to real-time processing capabilities. In fact, the constraints in their memory capacity prevent from loading the whole image in the RAM memory and block-based processing is required.

We assume that the objects of interest are mobile. First, assuming a static environment, the moving objects are identified through difference with respect to a reference image. A pixel of image k $Im_k(x,y)$ is considered part of a mobile object if $|Im_k(x,y) - Im_{ref}(x,y)| > T$, where T is a color threshold and $Im_{ref}(x,y)$ is the reference image. To reduce computer burden, images are divided in windows and if the number of pixels which color has changed is above NP , the window is considered with motion.

In case the color of the object of interest can be characterized, then a color-based segmentation is applied only to the windows with motion previously identified. For this operation the HSI color field is preferred in order to achieve higher stability of color with lighting changes. Then, an efficient 8-neighbours region-growing algorithm is used. Finally, the characteristics of the region of interest such as coordinates of the central pixel, region width and height are obtained. Figure 6 shows the results of each step over an image from a *CMUcam3* in which a fireman is segmented.



Fig. 6. Left) Object segmentation using motion. Right) Object segmentation using color.

The algorithm has been efficiently programmed so that the complete segmentation (the images are 352x288 pixels) takes 560 ms., 380 ms. of which are devoted to downloading the image from the internal camera buffer to the *CMUcam3* board memory.

6.1.2 Image distortions correction

In the next step, before transmitting the measurements for data fusion, each camera node corrects its own optical distortions, transforming them to the normalized pin-hole

projection. Let $P_i=[X_i \ Y_i \ Z_i]^T$ be the coordinates of a point in the environment expressed in reference frame local to camera i , F_i . Assuming an ideal pin-hole model, the normalized projection of P_i on the image plane of camera i is $p_i=[X/Z \ Y/Z]^T=[x_i \ y_i]^T$. After including lens radial and tangential distortions, the distorted point $p_i^d=[x_i^d \ y_i^d]^T$ is defined as follows:

$$p_i^d = d_i^r p_i + d_i^t \quad (17)$$

where d_i^r and d_i^t are simplified radial and tangential distortions terms as defined in the model described in (Heikkilä & Silven, 1997):

$$d_i^r = 1 + ar_i^2 + br_i^4 \quad d_i^t = \begin{bmatrix} 2cx_i y_i + d(r_i^2 + 2x_i^2) \\ c(r_i^2 + 2y_i^2) + 2dx_i y_i \end{bmatrix} \quad (18)$$

where $r_i^2=x_i^2+y_i^2$. Finally, assuming the skew factor is zero, the pixel coordinates on the image $p_i^p=[x_i^p \ y_i^p]^T$ are determined considering the focal length f and the coordinates of the principal point of the lens cc of camera i by using the following expression:

$$p_i^p = fp_i^d + cc \quad (19)$$

The internal calibration parameters -optical distortion parameters a , b , c and d , the focal distance f and the coordinates of the principal point of the lens cc - are considered known at each camera node. Consider p_i^p is the pixel coordinates of the centre of a region of interest segmented in the images. The correction is applied in two steps: obtain p_i^d using (19) and compute p_i using (17) and (18). For practical purposes (18) is usually approximated using x_i^d and y_i^d instead of x_i and y_i . Thus, $p_i=[x_i \ y_i]^T$ can be computed efficiently involving only two divisions and few products and sums. It is executed in the *Xbow* node itself.

Also, the position and orientation for each camera in a global reference frame are assumed known at each camera node. These 6 parameters -3 for camera position and 3 for orientation- are included in the measurements packets sent for data fusion so that it can cope with static and mobile cameras, for instance on very light-weight UAVs. The time stamps of the measurements are also included in these packets for synchronization.

6.1.3 Interface and synchronization modules

Several software modules were implemented on the *Xbow* mote. One of them implements the command interface with the *CMUcam3* using low-level *TinyOS* routines. The node commands the *CMUcam3* to start capturing images at a certain rate and to execute object segmentation to the captured images. For each image, the *CMUcam3* replies the characteristics of the region segmented (centre, width and height). Then, the distortion correction method described in Section 6.1.2 is applied. Finally, the resulting measurements are sent through the WSN for data fusion. It should be noted that the *Xbow* nodes can disable or enable the operation of the *CMUcam3* board, allowing active perception techniques such as those described in Section 5.

Another software module was devoted to synchronization among camera nodes. The method selected is the so-called *Flooding Time Synchronization Protocol (FTSP)* (Maróti et al., 2004). This algorithm establishes hierarchies among the WSN nodes. The leader node periodically sends a synchronization message. Each camera node that receives the message resends it following a broadcast strategy. The local time of each camera node is corrected

depending on the time stamp on the message and the sender of the message. The resulting synchronization error is of few milliseconds.

6.2 Some results

Figure 7Left shows a picture of one localization and tracking experiment. The objective is to locate and track mobile robots that follow a known trajectory, taken as ground truth. Figure 7Right depicts a scheme of an environment involving 5 camera nodes at distributed locations and with different orientations. The local reference frames of each of the camera are depicted. The global reference frame is represented in black.

In this Section the three data fusion methods presented are compared in terms of accuracy and energy consumption. Accuracy is measured as the mean error with the ground truth. For the consumption analysis we will assume that the energy dedicated by the *Xbow* node to execute any of the three data fusion algorithms is significantly lower than the energy devoted by a camera node to obtain observations. The latter includes the energy required for image acquisition and segmentation in the *CMUcam3* boards. The energy consumed by a camera node during an experiment is proportional to the number of measurements made.

In all the experiments the commands given to the robot to generate the motion were the same. The object locations are represented with dots in Fig. 7Right. In all the experiments the measurements computed by cameras 2 and 3 from $t=10$ s. to $t=25$ s. are considered lost and cannot be used for data fusion. The object locations within this interval are marked with a rectangle in Fig. 7Right.

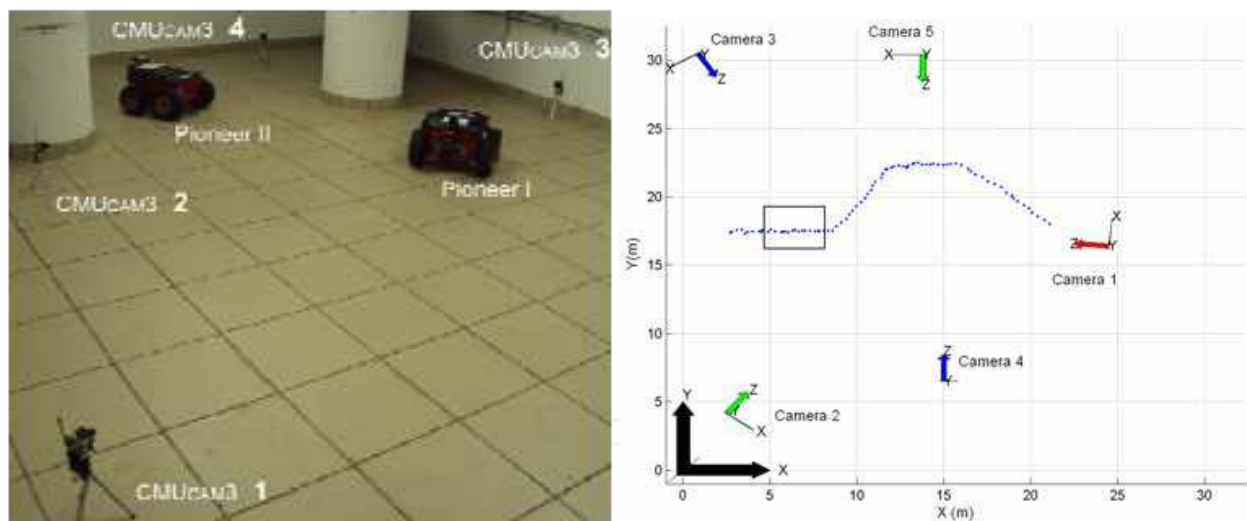


Fig. 7. Left) Object tracking experiment using 3 *CMUcam3* micro cameras. Right) Scheme of the environment involving 5 camera nodes.

Four different cases were analyzed: ML using cameras 1, 2 and 3; EIF using cameras 1, 2 and 3; EIF using the five cameras; and active perception with all the cameras. A set of ten repetitions of each experiment were carried out. Figures 8a-d shows the results obtained for axis X (left) and Y (right) in the four experiments. The ground truth is represented in black color and the estimated object locations are in red. In Figs. 8b-d the estimated 3σ confidence interval is represented in blue color. Table 1 shows the average of the mean error and the number of measurements used by each method.

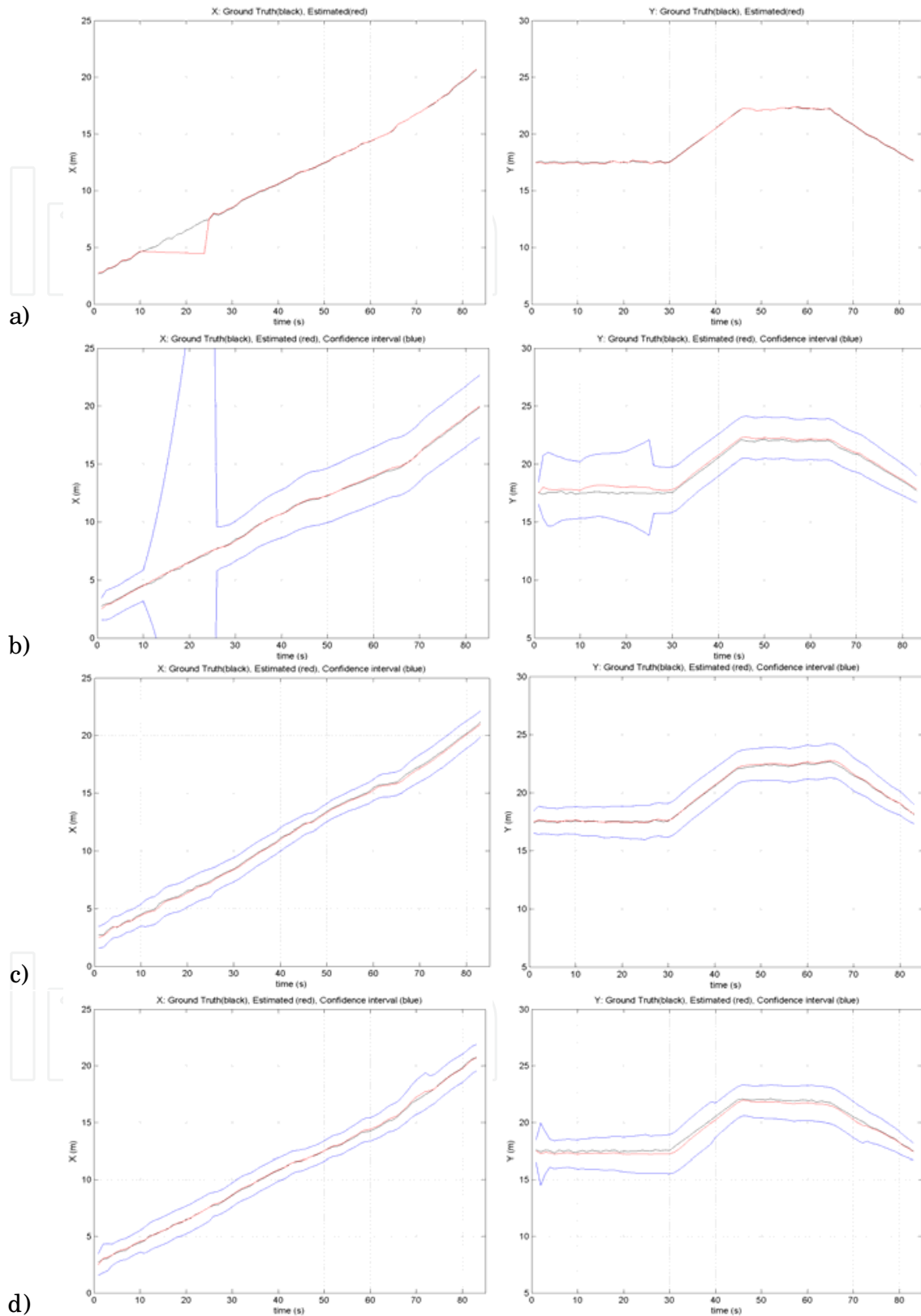


Fig. 8. Estimated X(Right) and Y(Left) location of the object: a) ML using cameras 1, 2 and 3, b) EIF with cameras 1, 2 and 3, c) EIF with the five cameras and, d) active perception.

	ML	EIF 3 cameras	EIF 5 cameras	Active Perception
Mean error (m.)	0.42	0.37	0.18	0.24
Number of measurements	225	225	395	239

Table 1. Average values of the mean error and number of measurements in the experiments.

In Fig. 8a it can be observed that the ML method performs quite well when the level of noise in the measurements is low. On the other hand, losses of measurements from cameras 2 and 3 originate important errors in the X coordinate of the estimated object location while measurements from camera 1 are enough to provide accuracy in the Y coordinate.

The EIF with cameras 1, 2 and 3 exhibits a more robust performance. The loss of measurements from cameras 2 and 3, prevents the EIF from having valid measurements for the X coordinate and thus, it relies on the system prediction model. Note that the covariance of the estimation in X increases gradually until measurements from camera 2 and 3 are again available, see Fig. 8b. Loss of measurements from cameras 2 and 3 have moderate effect in the confidence interval in Y. Globally the EIF achieved higher accuracy than the ML method in the experiments, see Table 1.

When all the cameras are fused, the estimation of the EIF is even more accurate: the 3σ confidence interval becomes narrower, see Fig. 8b,c, and the mean error becomes significantly lower, see Table 1. Loss of measurements from cameras 2 and 3 has negligible effect in the estimation because other cameras provide that information into the filter. On the other hand, using a higher number of cameras requires using often constrained in WSN applications.

The active perception method dynamically activates the camera nodes required to reduce the uncertainty and deactivates the non-informative camera nodes to save resources. The practical effect is that it obtains good object localization and tracking accuracy, see Fig. 8d, with a drastic reduction in the number of measurements used, see Table 1. In the experiments carried out the mean errors achieved by the active perception method were almost as good as those achieved by the EIF with 5 cameras (0.24 versus 0.18) but they needed 39.49% less measurements (239 versus 395).

Figure 9 shows the results in an experiment assuming a cost of $c(x_i,a)=0.2$ for all sensory actions. Figure 9Left shows which camera nodes are active at each time. It can be noted that camera 5 is the most informative one and is active during the whole experiment. In contrast, camera 2 is the less informative. Figure 9Right shows the estimated standard deviation for X (blue) and Y (red). The values of standard deviation are in the range 0.5-0.8 m. during the experiment except for the filter initialization. It can be noted that the standard deviation for X has a slight increase in the interval 10–25 s. originated by the lack of measurements from camera 2 and 3. In this experiment the mean error was 0.17 m. and the number of cameras used was 249.

The performance of the active perception is highly dependant on the values of the cost adopted to decide on the sensory action. The higher the cost, the higher has to be the information gain of an action to become advantageous. Figure 10 shows results obtained in an experiment using $c(x_i,a)=1.0$ for all sensory actions. It can be noted that the number of camera nodes active decreases significantly -only a total of 99 measurements were used in this experiment needing 74.93% less resources than EIF with 5 cameras- without much degradation in the standard deviation, which keeps in the range 0.6-1.3 m. In this experiment the mean error was 0.26 m.

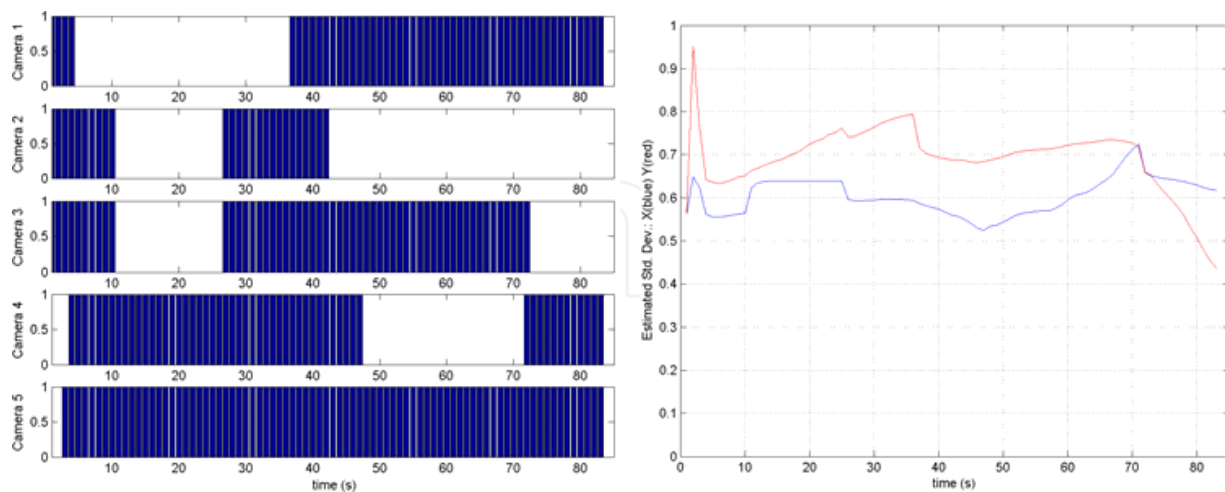


Fig. 9. Results in an experiment using $c(x_t, a) = 0.2$ for all sensory actions.

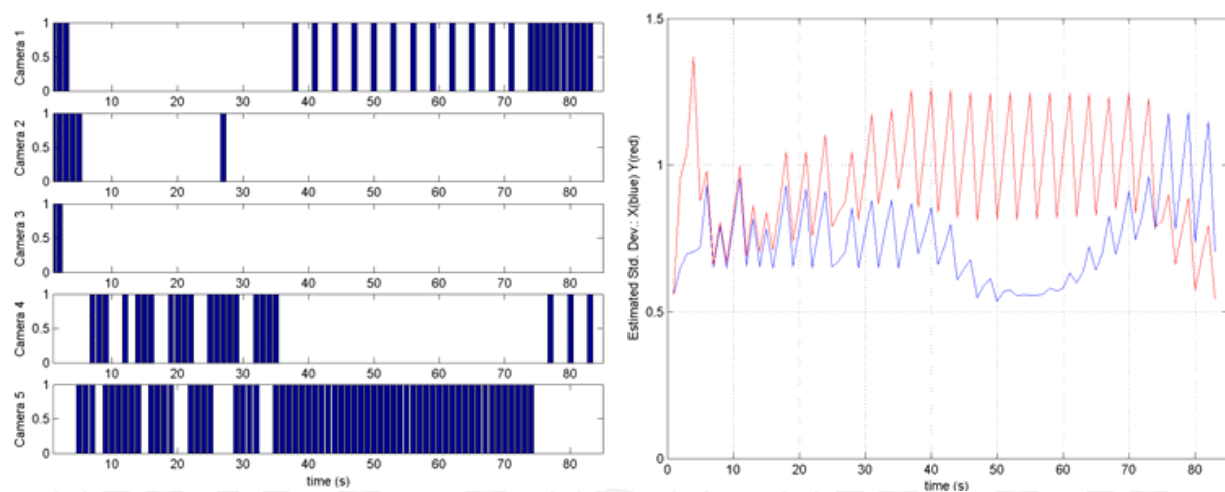


Fig. 10. Results in an experiment using $c(x_t, a) = 1.0$ for all sensory actions.

7. Conclusions

This chapter describes three efficient data fusion methods for localization and tracking with WSN comprising nodes endowed with low-cost cameras as main sensors. The approach adopted is a partially decentralized scheme where the images captured by each camera node are processed locally using segmentation algorithms in order to extract the location of the object of interest on the image plane. Only low-bandwidth data is transmitted through the network for data fusion.

First, a Maximum Likelihood technique that fuses camera observations in a very efficient way is described. ML carries out data fusion using only the information contained in the

measurements. It has good performance when the level of noise in the measurements is low but degrades with noisy measurements and particularly with lacks of measurements, for instance in cases of losses of WSN messages.

Then, an Extended Information Filter is proposed. Bayesian Filters compute the estimation based on measurements and observation and system models. We preferred EIFs instead of its dual EKF since the update stage of EIF is more efficient than EKF and thus it is more suitable when there are a high number of observations, such as it is our case, where a good number of low-cost camera nodes can be used. The uncertainty of the perception using EIF is reduced by using more camera nodes at the expense of requiring more resources such as energy, bandwidth and computer and memory capacity.

Finally, an Active Perception method based on a greedy algorithm balances between the information that can be obtained from a camera node and the cost of that information. The method dynamically activates the most-informative camera nodes required to reduce the uncertainty and deactivates the least-informative ones to save resources.

Several experiments with WSN comprising *Xbow* nodes and *CMUcam3* boards are used to compare the methods and illustrate their advantages and disadvantages.

The described methods have limited scalability with the number of camera nodes due to the computational and memory constraints of WSN nodes and limitations in the effective WSN bandwidth. The reliability to failures of the node performing the data fusion is also an important drawback. Decentralized data fusion can help to improve these issues. Efficient fully decentralized schemes suitable for camera-based WSN are object of current research.

8. References

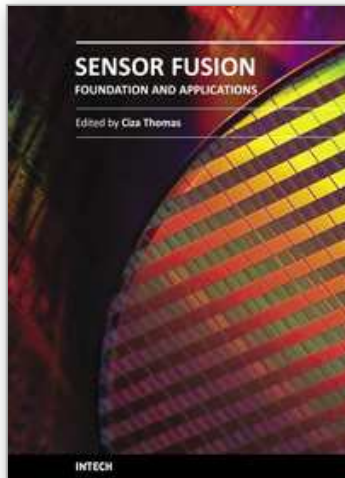
- Akyildiz, I.F.; Su, W.; Sankarasubramaniam, Y. & Cayirci, E. (2002). A Survey on Sensor Networks. *IEEE Communications Magazine*, Vol.40, No.8, (August 2002), pp. 102-114, ISSN 0163-6804
- Al-Karaki, J.N. & Kamal, A.E. (2004). Routing Techniques in Wireless Sensor Networks: a Survey. *IEEE Wireless Communications*, Vol.11, No.6, pp. 6-28, ISSN 1536-1284
- Amundson, I. & Koutsoukos, X. (2009). A Survey on Localization for Mobile Wireless Sensor Networks, *Proceedings of the Second International Workshop on Mobile Entity Localization and Tracking in GPS-less Environments*, pp. 235-254, ISBN 3-642-04378-X 978-3-642-04378-9, Orlando FL, USA, September 30, 2009
- Black, J. & Ellis, T. (2006). Multi Camera Image Tracking. *Image and Vision Computing*, Vol.24, No.11, (November 2006), pp. 1256-1267, ISSN 0262-8856
- Depenthal, C. & Schwendemann, J. (2009). IGPS - A New System for Static and Kinematic Measurements, *Proceedings of the 9th Conference on Optical 3D Measurement Techniques*, pp. 131-140, ISBN 978-3-9501492-5-8, Viena, Austria, July 1-3, 2009
- Gezici, S.; Zhi Tian; Giannakis, G.B.; Kobayashi, H.; Molisch, A.F.; Poor, H.V. & Sahinoglu, Z. (2005). Localization via Ultra-Wideband Radios. *IEEE Signal Processing Magazine*, Vol.25, No.4, (July 2005), pp. 70-84, ISSN 1053-5888
- Grewal, S. M.; Weill, L.R. & Andrews, A.P. (January 2007). *Positioning Systems, Inertial Navigation, and Integration*, Wiley-Interscience, ISBN 0470041900

- Grocholsky, B.; Keller, J.; Kumar, V. & Pappas, G. (2006). Cooperative Air and Ground Surveillance, *IEEE Robotics & Automation Magazine*, Vol.13, No.3, pp. 16-25, ISSN 1070-9932
- Hanssmann, M.; Rhee, S. & Liu, S. (2008). The Applicability of Wireless Technologies for Industrial Manufacturing Applications Including Cement Manufacturing, *Proceedings of the IEEE Cement Industry Technical Conference 2008*, pp.155-160, ISBN 978-1-4244-2080-3, Miami FL, USA, May 18-22, 2008
- Heikkila, J. & Silven, O. (1997). A Four-step Camera Calibration Procedure with Implicit Image Correction, *Proceedings of the 1997 Conference on Computer Vision and Pattern Recognition*, pp. 1106, ISBN 0-8186-7822-4, San Juan, Puerto Rico, June 17-19, 1997.
- Kaelbling, L.P.; Littman, M.L. & Cassandra A.R. (1998). Planning and acting in partially observable stochastic domains. *Artificial Intelligence*, Vol.101, No.1-2, pp. 99–134, ISSN 0004-3702
- Maróti, M.; Kusy, B.; Simon G. & Lédeczi, A. (2004). The Flooding Time Synchronization Protocol, *Proceedings of the ACM Second International Conference on Embedded Networked Sensor Systems*, pp. 39-49, ISBN 1-58113-879-2, Baltimore MD, USA, November 3-5, 2004
- Mohammad-Djafari, A. (1997). Probabilistic Methods for Data Fusion, *Proceedings of the 17th International Maximum on Entropy and Bayesian Methods*, pp. 57-69, ISBN 978-0-7923-5047-7, Boise Idaho, USA, August 4-8, 1997
- Nath, B.; Reynolds, F. & Want, R. (2006). RFID Technology and Applications. *IEEE Pervasive Computing*, Vol.5, No.1, pp 22-24, ISSN 1536-1268
- Polastre, J.; Szewczyk, R.; Mainwaring, A.; Culler D. & Anderson, J. (2004). Analysis of Wireless Sensor Networks for Habitat Monitoring, In: *Wireless Sensor Networks*, C. S. Raghavendra, K.M. Sivalingam, T. Znati, (Eds.), pp. 399-423, Kluwer Academic Publishers, ISBN 1-4020-7883-8, Norwell, MA, USA
- Rice, J. (April 2006). *Mathematical Statistics and Data Analysis*. (3rd ed.), Brooks/ Cole, ISBN 0534399428
- Sandhu, J. S.; Agogino, A.M. & Agogino A.K. (2004). Wireless Sensor Networks for Commercial Lighting Control: Decision Making with Multi-agent Systems, *Proceedings of the AAAI Workshop on Sensor Networks*, pp. 88-89, ISBN 978-0-262-51183-4, San Jose CA, USA, July 25-26, 2004
- Shaferman, V.; & Shima, T. (2008). Cooperative UAV Tracking Under Urban Occlusions and Airspace Limitations, *Proceedings of the AIAA Conf. on Guidance, Navigation and Control*, , ISBN 1-56347-945-1, Honolulu, Hawaii, USA, Aug 18-21, 2008
- Thrun, S.; Burgard, W. & Fox, D. (September 2005). *Probabilistic Robotics*. The MIT Press, ISBN 0262201623, Cambridge, Massachusetts, USA
- Wark, T.; Corke, P.; Karlsson, J.; Sikka, P. & Valencia, P. (2007). Real-time Image Streaming over a Low-Bandwidth Wireless Camera Network, *Proceedings of the Intl. Conf. on Intelligent Sensors*, pp. 113-118, ISBN 978-1-4244-1501-4, Melbourne, Australia, December 3-6, 2007

Zanca, G.; Zorzi, F.; Zanella, A. & Zorzi, M. (2008). Experimental Comparison of RSSI-based Localization Algorithms for Indoor Wireless Sensor Networks, *Proceedings of the Workshop on Real-World Wireless Sensor Networks*, pp. 1-5, ISBN 978-1-60558-123-1, Glasgow, UK, April 1, 2008

IntechOpen

IntechOpen



Sensor Fusion - Foundation and Applications

Edited by Dr. Ciza Thomas

ISBN 978-953-307-446-7

Hard cover, 226 pages

Publisher InTech

Published online 24, June, 2011

Published in print edition June, 2011

Sensor Fusion - Foundation and Applications comprehensively covers the foundation and applications of sensor fusion. This book provides some novel ideas, theories, and solutions related to the research areas in the field of sensor fusion. The book explores some of the latest practices and research works in the area of sensor fusion. The book contains chapters with different methods of sensor fusion for different engineering as well as non-engineering applications. Advanced applications of sensor fusion in the areas of mobile robots, automatic vehicles, airborne threats, agriculture, medical field and intrusion detection are covered in this book. Sufficient evidences and analyses have been provided in the chapter to show the effectiveness of sensor fusion in various applications. This book would serve as an invaluable reference for professionals involved in various applications of sensor fusion.

How to reference

In order to correctly reference this scholarly work, feel free to copy and paste the following:

J.R. Martinez-de Dios, A. Jimenez-Gonzalez and A. Ollero (2011). Localization and Tracking Using Camera-Based Wireless Sensor Networks, Sensor Fusion - Foundation and Applications, Dr. Ciza Thomas (Ed.), ISBN: 978-953-307-446-7, InTech, Available from: <http://www.intechopen.com/books/sensor-fusion-foundation-and-applications/localization-and-tracking-using-camera-based-wireless-sensor-networks>

INTECH
open science | open minds

InTech Europe

University Campus STeP Ri
Slavka Krautzeka 83/A
51000 Rijeka, Croatia
Phone: +385 (51) 770 447
Fax: +385 (51) 686 166
www.intechopen.com

InTech China

Unit 405, Office Block, Hotel Equatorial Shanghai
No.65, Yan An Road (West), Shanghai, 200040, China
中国上海市延安西路65号上海国际贵都大饭店办公楼405单元
Phone: +86-21-62489820
Fax: +86-21-62489821

© 2011 The Author(s). Licensee IntechOpen. This chapter is distributed under the terms of the [Creative Commons Attribution-NonCommercial-ShareAlike-3.0 License](#), which permits use, distribution and reproduction for non-commercial purposes, provided the original is properly cited and derivative works building on this content are distributed under the same license.

IntechOpen

IntechOpen